BACHELOR

Influence of mechanical history on the nano-porosity of glassy-systems

van den Ameele, Noël C.

Award date:
2024

Influence of mechanical history on the nano-porosity of glassy-systems

Bachelor End Project: Mechanical Engineering

Department Processing and Performance (Group Hütter) - Q4 (2024)

Full Name	Student ID
Noël van den Ameele	1613499

Tutor: Kostas Steiakakis, MSc
BEP coordinator: Markus Hütter, dr.sc.nat.

Eindhoven, July 12, 2024

Contents

List of symbols

Symbol	Dimension	Unit	Unit abbreviation
l	Length	Angstrom	Å
t	Time	nanosecond	ns
T	Temperature	Kelvin	K
P	Pressure	bar	bar
m	Mass	gram per mole	g/mol
ε	Strain	[-]	[-]
$\dot{\varepsilon}$	Strain rate	inverse second	s^{-1}
r	Radius	Angstrom	Å
n_{vox}	Number of voxels	[-]	[-]
n_{cav}	Number of cavities	[-]	[-]
V	Volume	Angstrom cubed	$Å^3$
V_{tot}	Total accessible volume	Angstrom cubed	$Å^3$
$V_{cav,i}$	Volume per cavity	Angstrom cubed	$Å^3$
$\bar{V}_n$	Numerical average volume	Angstrom cubed	$Å^3$
$\bar{V}_w$	Weighted average volume	Angstrom cubed	$Å^3$
$\mathcal{U}$	Potential energy	kilo calories per mole	$kcal/mol$
N	Number of particles	[-]	[-]
r^N	Set of positions	[-]	[-]
β	Coldness	Inverse Joule	J^{-1}
μ	Chemical potential	kilo calories per mole	$kcal/mol$
ρ	Density	gram per mole Angstrom cubed	$g/mol\dot{A}^3$
Θ	Fugacity constant	[-]	[-]
Λ	Brogli wave length	Angstrom	Å
s	Atom position vector	Angstrom	Å
V_{STP}	Volume of gasses at STP	Angstrom cubed	$Å^3$
V_{cell}	Volume of simulation cell	Angstrom cubed	$Å^3$
λ	Stretch factor	[-]	[-]
$\mathbf{F}$	Deformation tensor	[-]	[-]
$\vec{x}$	Deformed position vector	Angstrom	Å
$\vec{X}$	Original position vector	Angstrom	Å

Constant	Value	Unit abbreviation
Boltzmann constant (k_b)	1.380649e-23	$m^2kgs^{-2}K^{-1}$
Planck's constant (h)	6.62607015e-34	m^2kg/s

1 | Introduction

In the world of material science, polymers stand out with their individual versatility and variety of applications due to their unique structural properties which arise from their chemistry and micro-structure [1]. Based on their micro-structure, polymeric materials can be divided into semi-crystalline and amorphous (or glassy) polymers. Polymers of which the chains have the ability to partially arrange in a structured manner forming closely-packed domains (crystalline formations) belong to the first category while polymers whose molecular structure are not able to do that belong to the second.
Glassy materials are characterised by high nano-scopic free volume (nano-porosity) [2] between their chains in which diffusing gas molecules can reside. Processing a polymer changes the relative positions of its chains due to mechanical and thermal stress which in turn could affect the nano-porosity and subsequently the solubility of penetrant gases in their matrix. Depending on the specific application of the polymer, the solubility of gas molecules might be desirable, or not. As an example, for food storage the gas solubility of a container should be low, such that the food is not affected by gases diffusing through the container. But a polystyrene membrane or filter should be nano-porous such that (specific) molecules can diffuse through and separate [3].
Polystyrene [4], a widely used thermoplastic polymer, is of great industrial significance due to its relatively high tensile strength, making it an excellent material for a variety of applications. Below its glass transition temperature T_g (glass transition temperature), where it remains rigid and brittle, atactic polystyrene has an amorphous structure made up of repeating styrene monomer units. This amorphous structure arises because the irregular chain architecture prevents crystallization upon cooling below the T_g. This amorphous structure of atactic polystyrene has a relatively low gas barrier [2], allowing molecules such as oxygen and methane to enter and reside in its nano-cavities.

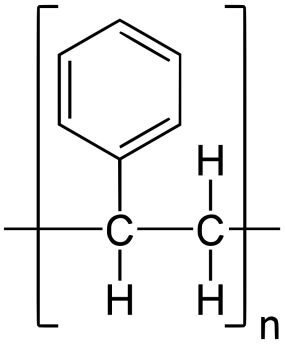

Figure 1.1: A polystyrene repeating unit

Different molecules can also solubilize differently according to their relative sizes and distinct properties [5]. Mechanical deformation is expected to affect the solubility of penetrant gases in the polystyrene matrix because it alters the distribution of their accessible volume in the matrix and the geometric characteristics of the cavities they reside in.
In this report, the structure of these cavities and the molecular solubility in polystyrene after the application of different deformations (compression, elongation and shear) under 0.05 strain will be studied using Molecular Dynamics (MD) simulations [6] as a computational method. These are basic deformations which can represent a simplified version of a mechanical load during manufacturing and service. The final applied strain is chosen to be 0.05, because polystyrene is a brittle material and the deformations should be considered in the elastic domain in order to be strain-rate independent. Such properties as the nano-porosity and resulting molecular gas diffusion inside polystyrene have been studied using experimental methods extensively [7], but this is generally more expensive and time-consuming. By using computational MD-simulations, the resulting matrix geometries due to the different deformations can be compared equitably. The potential gaseous penetrants for which the accessible volume and solubility in the polystyrene matrix will be studied are: methane, nitrogen, oxygen and hydrogen, because these are common gases in the service environments of polymeric materials.

2 | Methodology

To properly analyze the cavities and quantify the solubility of penetrants, a Molecular Dynamics simulation [6] with a geometric cell of approximately 38x38x38 Å with periodic boundary conditions is set up to compare the geometric state of the cavities before and after each deformation. The configuration of the atactic polystyrene in this box consists of four individual chains each with 80 monomers, with a molecular weight of 8360 g/mol.

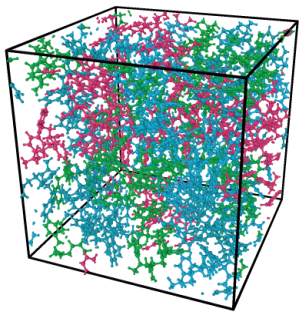

Figure 2.1: Initial state of the polystyrene matrix with each of the chains colour coded

The program Large-scale Atomic/Molecular Massively Parallel Simulator (LAMMPS) is used for all simulations with the Optimized Potentials for Liquid Simulations - All Atom (OPLS-AA) force field [8] such that bonded and non-bonded interactions are parameterised according to this OPLS-AA force field. Partial charges are assigned to the atoms according to this same force field.
To compare the cavity geometries and the solubility of the gaseous penetrants equitably before and after the different applied deformations, a specific simulation architecture (subsection 2.1) was set up. The different states of the polystyrene correspond to the initial equilibrated pre-deformation run which represents the steady and undeformed state of the polystyrene matrix and three deformation runs which represent the steady-state of the polystyrene after the different deformations have been applied to the previously equilibrated polystyrene configuration in which the 0.05 total strain is imposed.

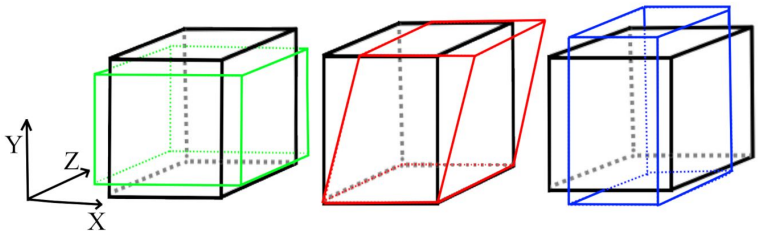

Figure 2.2: The prospective deformations, from left to right, elongation, shear and compression in a Cartesian coordinate system

2.1 | Simulation architecture

Equilibration of the polystyrene matrix is reached by imposing an initial NPT-run which calibrates the system at a temperature of 300 K and a pressure of 1 bar. The full NPT-run lasts for 1 ns and the temperature and pressure are controlled by a Nose-Hoover barostat and Nose-Hoover thermostat respectively [9]. After the pressure has been equilibrated, a NVT-run controlled in the same manner takes over to fully "relax" the system and to reach the final equilibrated and undeformed state at 300 K. This NVT-run lasts in total 2 ns. In the last nanosecond of the NVT-run, configurations are saved in Cartesian coordinates with a frame-saving frequency of 1 every ps.
The equilibration is assumed to be reached when the total energy has converged to its plateau value (Figure 3.1). Small fluctuations in energy, temperature and volume are expected around their desired values, attributed to the Nose-Hoover controllers.

The properties of the configurations from the equilibrium stage without any deformation will be compared to the relevant properties gathered from the deformation runs. The final state of the pre-deformation run is used as the initial state for each of the three deformation runs. During which 0.05 total strain compression, elongation and shear deformation are applied to the polystyrene respectively.
The different deformations (elongation, shear and compression) Figure 2.2 are all applied by exacting a strain rate of 1e7 s^{-1} for 500 ps which results in a total strain of 0.05. This follows from the simple formula:

$$\varepsilon = \dot{\varepsilon} \cdot t \tag{2.1}$$

The polystyrene matrix can be assumed to be in an elastic state [10] since the yield point of polystyrene with a comparable strain rate is around 0.2 strain.
After the strain has been applied it is held constant for the rest of the duration of the runs.
The configuration sampling and analysis during the deformation runs is conducted with the same time-span and frequency as the undeformed run. The polymeric geometry during the undeformed and deformation runs will be compared to see if the mechanical history of the polystyrene has an effect on accessibility and the potential solubility of molecular penetrants in the matrix.

2.2 | Cavity searching

Cavity searching in the context of these molecular dynamics simulations is done by executing a separate script on the atomic positional data of each time-step of the initial LAMMPS-simulation. For each designated configuration, the simulation box is subdivided into a grid of equally-sized cuboid voxels. After which, a hit-or-miss algorithm assesses whether a spherical probe, of which the radius mirrors the kinematic radius of a penetrant molecule, can be positioned at the voxel centers without overlapping with the atoms of the polystyrene matrix.

	Methane CH_4	Nitrogen N_2	Oxygen O_2	Hydrogen H_2
Atomic radius in [Å]	1.900	1.820	1.730	1.445

Table 2.1: The atomic radii used for the probes

This check is executed through calculations of the distances between the voxels center points to the surrounding atoms. Voxels for which no overlap is taking place are marked as accessible volume to the centre of the penterant. These empty voxels are then aggregated into cavities, grouped by their geometric proximity. Thus each cavity consists of n_{vox} voxels.

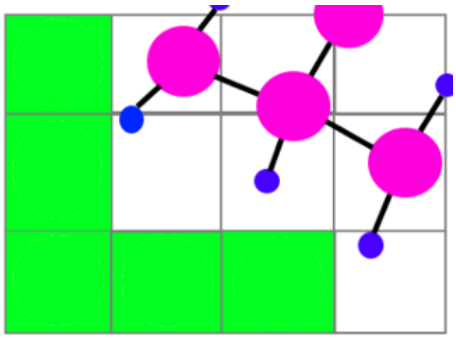

Figure 2.3: Visualization of the cavity-finding algorithm. The pink (carbon) and blue (hydrogen) circles represent the polystyrene chain while the green voxels represent the voxels where the center of the oxygen penetrants can be placed without overlapping with polystyrene atoms.

The process of identifying penetrant-accessible and free volume becomes more accurate as the resolution increases using a denser grid, subdividing the cell into smaller voxels. However, a larger resolution analysis also takes up more computational power and time. This is the case, because the number of voxels that need to be investigated through the algorithm increases cubically with the resolution.
The optimal resolution had to be determined first, before the MD-runs could be analyzed by the cavity searching algorithm. This is done by consulting four metrics. The first metric is the number of cavities

n_{cav} (Figure 2.4a) in the configuration. Secondly, the total accessible volume V_{tot} (Figure 2.4b), for the configuration housing n_{cav} cavities is calculated by summing the volumes of each individual cavity, represented as $V_{cav,i}$. This is done for a certain given molecular radius indicated in Å.

$$V_{tot} = \sum_{i=1}^{n_{cav}} V_{cav,i} \tag{2.2}$$

Thirdly, the numerical average volume $\bar{V_n}$ (Figure 2.4c) of the cavities is calculated by dividing the total cavity volume by the number of cavities.

$$\bar{V_n} = \frac{V_{tot}}{n_{cav}} \tag{2.3}$$

Lastly, the weighted average volume of the cavities $\bar{V_w}$ (Figure 2.4d) is also consulted because it becomes apparent that there is a big variation in the cavity volumes. The weighted average volume takes these disparities into account.

$$\bar{V_w} = \sum_{i=1}^{n} \frac{V_{cav,i}^2}{V_{tot}} \tag{2.4}$$

To establish this optimal resolution, the same initial configuration as for the molecular dynamics simulation is used to run and test different resolutions. The radius of the probe for this test is 1.73 Å, the radius of an oxygen molecule. The three aforementioned metrics are evaluated across voxel volumes ranging from 0.05425 Å^3 to 0.00085 Å^3.

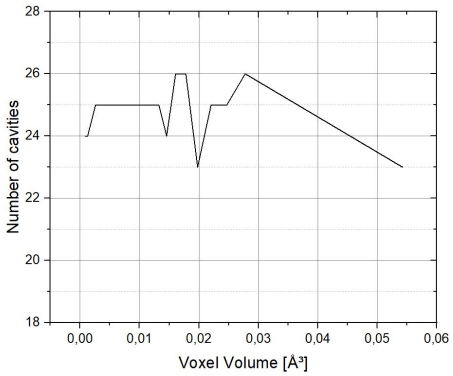

(a) Number of cavities

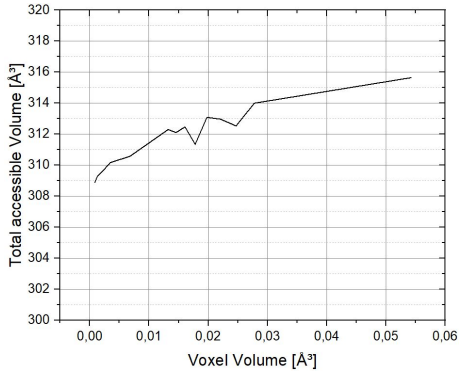

(b) Total free accessible volume $[A^3]$

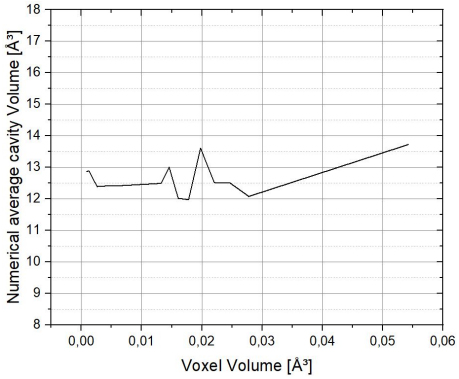

(c) Numerical average cavity volume $[A^3]$

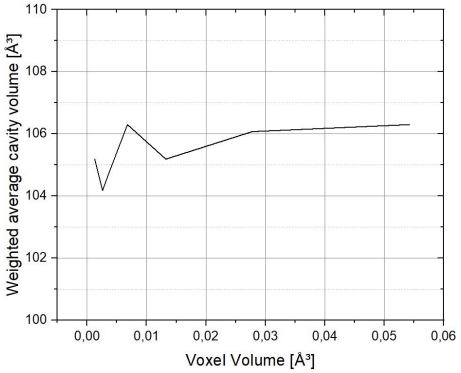

(d) Weighted average cavity volume $[A^3]$

Figure 2.4: The four metrics used to find the optimal voxel resolution

Analysis reveals that as the voxel size decreases, the total accessible volume Figure 2.4b initially seems to be overestimated because of the coarser resolution. Similarly, the abrupt (but small) changes in the numerical average volume Figure 2.4c is caused by the emergence and disappearing of a few small cavities, because they are assimilated or split from the bigger ones. This behaviour can be deduced from Figure 2.4a where the number of cavities in the configuration shifts between 23 and 26 until it seems to be converging

to a total of 24. The weighted average volume $\bar{V}_w$ takes this into account however, and this metric remains very stable for all the tested resolutions.
Ultimately, as a good trade-off for efficiency and precision, the desired grid resolution is identified with the voxel volume at 0.0542 Å^3. Even though this is the highest voxel volume tested, all the metrics only have very slight deviations in accuracy from this resolution onwards while a higher resolution would result in unreasonable computational costs. As such, this resolution is deemed to be the appropriate balance between computational cost and accurate cavity mapping during the following molecular dynamics simulations.

2.3 | Isotropy

One general concern is that the results for the cavity-geometry analysis would be dependent on the direction of the applied deformation which would influence the metrics described in subsection 2.2. The suggested framework would not be reliable in this case because of the anisotropy of the polystyrene matrix. To examine this notion, additional MD deformation runs of the 0.05 elongation and compression both in the y- and z-direction are simulated along the ones in the x-direction to show the effect of the deformation direction on the oxygen accessible free volume (Equation 2.2). This is done by using the cavity searching algorithm from subsection 2.2 as discussed previously.

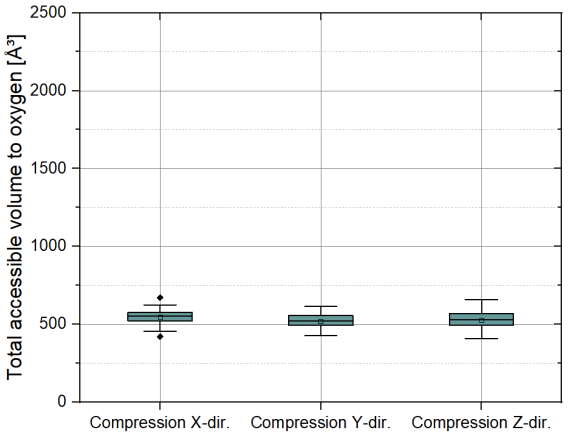

Figure 2.5: Cavity analysis results for different compression directions

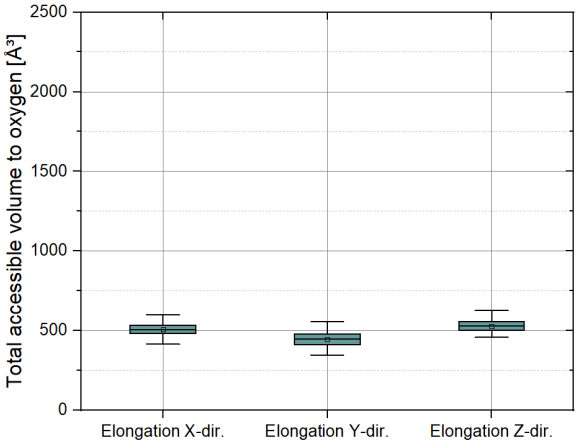

Figure 2.6: Cavity analysis results for different elongation directions

The graphs clearly indicate that the the mean and variation of the accessible volume to oxygen does not depend on the direction in which the polystyrene matrix is loaded. This means that for the intents and purposes of this report the polystyrene matrix is considered isotropic and therefore the results for each of the different deformation runs can be assumed to hold for any loading direction perpendicular to the coordinate system.

2.4 | Grand Canonical Monte Carlo solubility simulations

To find a computational estimate of the solubility of different penetrant molecules in the polystyrene, a Grand Canonical Monte Carlo (GCMC) simulation [11] is performed on ten configurations each sampled from the equilibration prior to the deformation and deformation runs. This way, the solubility of the different gases (methane, nitrogen, oxygen and hydrogen) can be compared before and after the deformations have been applied. The GCMC simulation works as follows: The configuration of the polystyrene exchanges molecules with an imaginary ideal gas reservoir at a specified temperature and pressure. For each step of the GCMC-run three moves are allowed, the introduction of the penetrant molecule at a random location in the polystyrene matrix, the removal of an existing penetrant that "returns" in the imaginary gas tank, or the displacement of a penetrant in the matrix. After a move is assumed, the energy difference due to the addition, removal, or displacement of the molecule is calculated to determine the acceptance of the move based on the Metropolis criterion. This Metropolis criterion is constructed as a Markov process where the probability of a Monte Carlo move happening is proportional to the Boltzmann factor:

$$\exp[-\beta \mathcal{U}(\mathbf{r}^N)] \tag{2.5}$$

where $\mathcal{U}(\mathbf{r}^N)$ represents the potential energy of a system of N particles, in which r^N denotes the set of positions of all N particles in the system. In this equation β, the coldness, is defined as

$$\beta = \frac{1}{k_b T} \tag{2.6}$$

where k_b is the Boltzmann constant and T stands for the temperature which is in this case set at 300 K. The chemical potential is given as:

$$\mu = k_b T \ln \rho \Lambda^3 = k_b T \ln \frac{\Theta P \Lambda^3}{k_b T} \tag{2.7}$$

where P is the pressure of the gas tank at 1 atm with Λ being the "de Broglie" wavelength and ρ being the gas-tank density. Θ represents the fugacity coefficient which in this case, is set to 1.
The "de Broglie" wavelength Λ is characterized by the equation:

$$\Lambda = \sqrt{\frac{h^2}{2\pi m k_b T}} \tag{2.8}$$

where h is Plank's constant and m is the mass of the penetrant molecule.
The chemical potential μ and the Boltzmann factor $\exp[-\beta \mathcal{U}(\mathbf{r}^N)]$ are used to predict the probability of a new particle going from the imaginary ideal gas reservoir to settling into the polystyrene matrix. The probability is given as:

$$\text{acc}(N \to N+1) = \min\left[1, \frac{V}{\Lambda^3 (N+1)} \exp\left\{\beta\left[\mu - \mathcal{U}(N+1) + \mathcal{U}(N)\right]\right\}\right] \tag{2.9}$$

while the removal of a particle is accepted with the probability

$$\text{acc}(N \to N-1) = \min\left[1, \frac{\Lambda^3 N}{V} \exp\left\{-\beta\left[\mu + \mathcal{U}(N-1) - \mathcal{U}(N)\right]\right\}\right]. \tag{2.10}$$

.
An existing particle in the polystyrene simulation cell is allowed to move with the probability

$$\text{acc}(s \to s') = \min\left(1, \exp\left\{-\beta\left[\mathcal{U}(s'^N) - \mathcal{U}(s^N)\right]\right\}\right). \tag{2.11}$$

where s represents the systems state.
By using a large number of steps, a good estimate of the potential solubility of the penetrant molecules can be estimated. Because the relative chemical potential between the molecules inside the imaginary gas tank and the polystyrene matrix is very much dependent on the the properties of the penetrant molecule itself, it is expected that there will be a considerable discrepancy between the different molecular solubilities.
As discussed in subsection 2.1, the GCMC-simulation is performed on 10 configurations each 100 ps apart during the last ns of the different deformation runs. 25,000 GCMC moves are prescribed on these configurations for each of the molecular penetrants. The solubility of these molecular penetrants inside of the different states of the polystyrene is described by the fraction of the ideal gas volume under STP (standard temperatue and pressure) conditions for each of the gaseous molecules over the simulation cell volume as a unitless metric.

3 | Molecular Dynamics simulation results

The following graphs depict the energy, temperature and volume during the undeformed and deformation runs. As previously described in subsection 2.1, the undeformed configurations are equilibrated with a NPT-run and consecutive NVT-run both lasting 1 ns while during the latter the cavity analysis (CA) configurations and solubility (GCMC) configurations are sampled. The deformation runs have as an initial state the last configuration of the undeformed run. The different stages of the simulation are indicated. First the NVT-deformation run deforms the matrix in the X-directions (XY-plane for the shear deformation). Then in the following NVT-run the matrix is equilibrated again such that the necessary configurations can be sampled in the last ns of each of the runs.

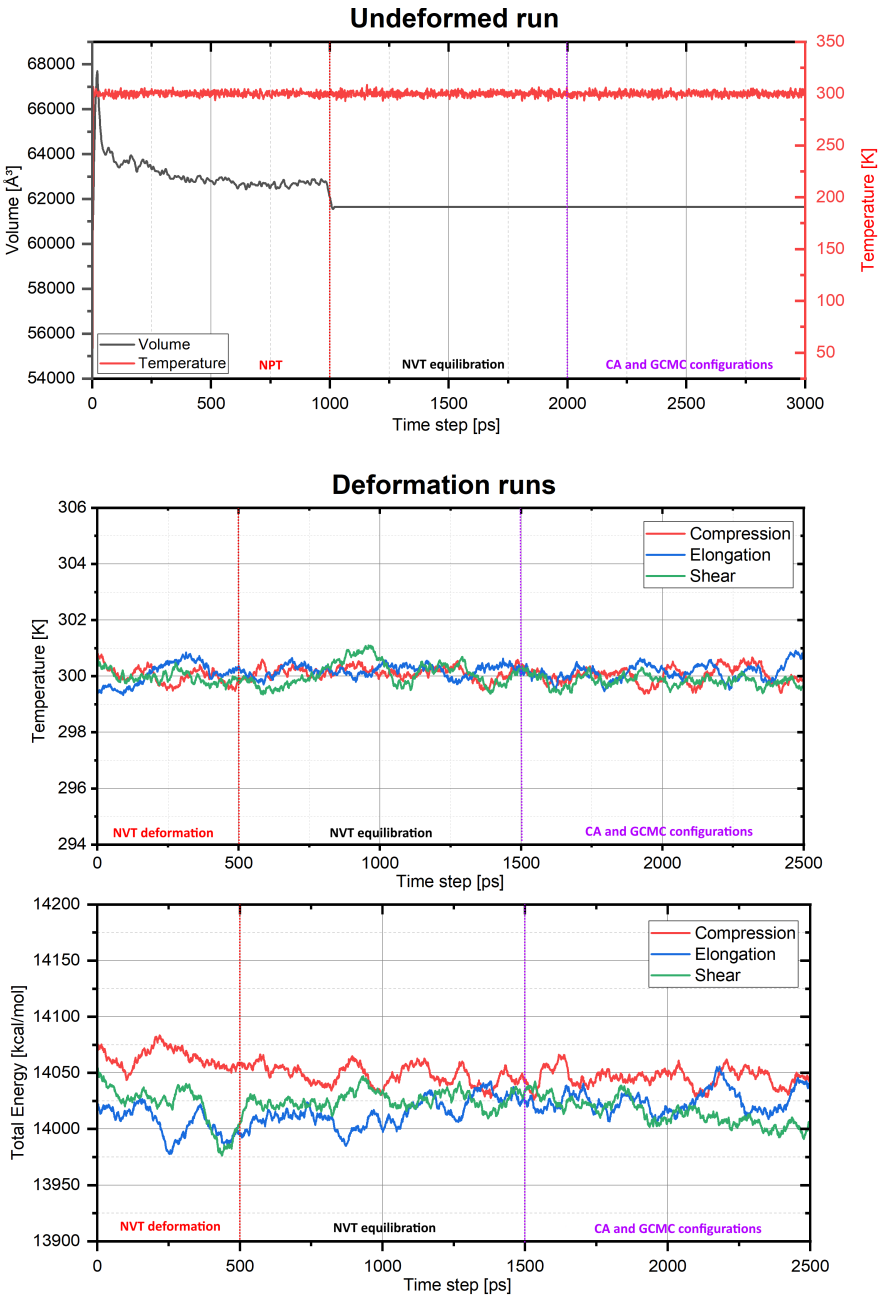

Figure 3.1: Volume [Å^3], Total energy [kcal/mol] and Temperature [K] plotted against time for each of the runs. The initial NPT and NVT-deformation for the undeformed and deformed runs respectively are indicated in red above the x-axis. The equilibration-run is indicated in black and the time-span of the configuration sampling is indicated in purple.

In the initial equilibration NPT-run the energy and volume spike to garner a steady-state for the polystyrene matrix after which the volume decreases gradually until it is completely fixed by the NVT-run. In this transition the temperature remains constant at the desired 300 K with a standard deviation less than 1 K which indicates the matrix is in a thermal equilibrium. After the system fully "relaxes" in this NVT-equilibration the configurations are taken. The state of the deformation configurations is assumed to be equilibrated because there is very little variation also in the temperature readings after the deformations have been applied. The average standard deviation of the energies is 13,807 kcal/mol while the average standard deviation of the temperatures is 0.33 K. So, in all the runs the energies and temperatures have plateaued enough such that the sampled configurations are considered to be representative of the imposed temperature and pressure. With the configurations being trustworthy for the comparison, the results can be used to quantify the cavity geometry and penetrant solubility reliably.

4 | Cavity analysis

Using the cavity searching algorithm introduced in subsection 2.2, the cavity geometry of the configurations of the undeformed state and deformed states can be analyzed. The cavity geometries shown in Figure 4.1 are the final states of each respective run for oxygen accessible volume.These configurations are sampled from the runs with the simulation architecture discussed in subsection 2.1 and deemed as equilibrated and trustworthy in section 3.
Between all the visualizations it can be stated that the cavity geometry is altered significantly after each of the deformations compared to the undeformed equilibrium state. It seems that the compressed configuration shown in Figure 4.1b has the biggest cavities while the sheared configuration in Figure 4.1d has more equivalently sized cavities. But this only holds for the configurations shown in Figure 4.1 which are the first of a hundred saved configurations for each different state. The cavity geometry changes significantly through the 1 ns in which the configurations are saved because of the vibrational movement of the individual polystyrene chains [12]. Ten configurations of oxygen accessible cavity geometry can be seen in Appendix A where it becomes clear that the cavity geometry changes throughout time, especially considering smaller cavities (subsubsection 4.2.3).
The metrics from subsection 2.2 which are plotted against time in Figure 4.1d shows these fluctuations in the number of cavities and accessible volume for the different penetrant molecules. So, even though Figure 3.1 shows that the MD simulation runs sample thermally equilibrated configurations, the cavity geometries can still evolve over time.

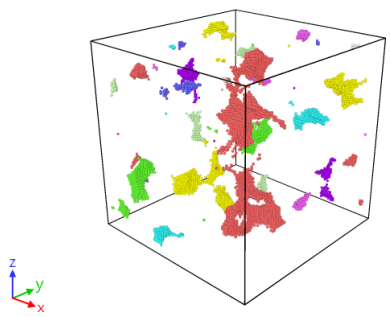

(a) Cavity geometry in the undeformed state

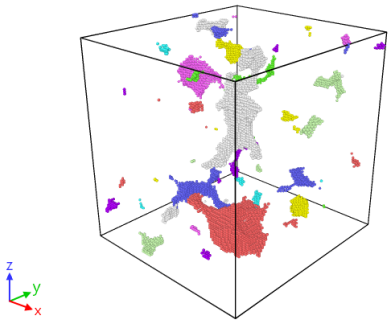

(b) Cavity geometry after compression

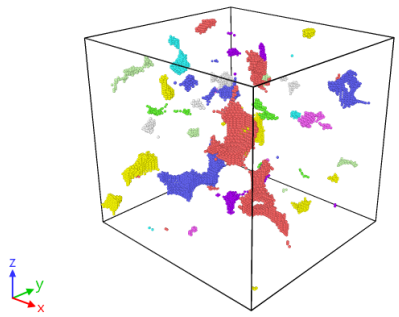

(c) Cavity geometry after elongation

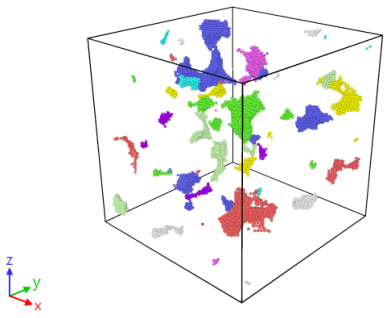

(d) Cavity geometry after shear

Figure 4.1: The geometry state of the cavities after each respective MD simulation

4.1 | Cavity metrics throughout simulation time

Below three of the discussed metrics in subsection 2.2 are plotted against simulation time after the shear deformation run with the strain held. The different metrics are discussed regarding the molecular penetrants: methane, nitrogen, oxygen and hydrogen. As expected, because hydrogen is the smallest molecule compared to the others, it has the most number of cavities, highest total accessible volume and

highest weighted average cavity volume. The accessible volume and number of cavities is in direct relation with the size of the molecules showcased in Table 2.1. This is logical, because the smaller the penetrant radius, the greater the chance to find more accessible volume in the polystyrene matrix. This is also reflected in the number of cavities metric, since smaller penetrants are more likely to have completely new cavities accessible to it. Volume not accessible to methane could potentially be accessible to hydrogen for example.
There are significant fluctuations noticeable from Figure 4.4 in the total accessible volume, especially in the number of cavities because of chain movement caused by thermal energy and inter-atomic forces [12]. These movements cause cavities to merge and split constantly, especially with smaller cavities which are sometimes prone to disappear altogether because a moving chain now blocks the previously accessible volume. So, even though the configurations are equilibrated properly the cavity geometry still evolves over time. The total accessible volume compared to the number of cavities remains stable throughout the simulation time (Figure 4.4) showing that cavity merging and splitting happens far more than cavity appearance and disappearance due to polymeric chain movements.
These observations also hold true for the other undeformed and deformed configurations. It could be argued however that these smaller cavities combining and splitting are not relevant for the solubility and diffusivity of the penetrant gases because of the incredibly low chance of a molecular penetrant actually visiting in them. Hereafter, a small cavity is defined as one with a volume of 3 $Å^3$ or less based on visual analysis otherwise it is mentioned as "big". In Figure 4.7 the number of cavities accessible to oxygen which are categorized by size are shown for the different types of runs.

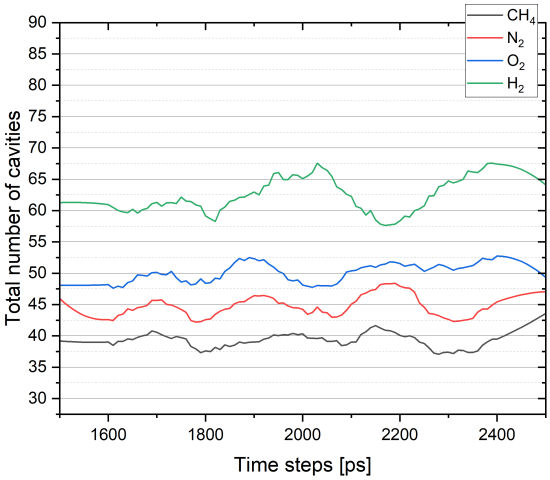

Figure 4.2: Number of cavities in the sheared matrix

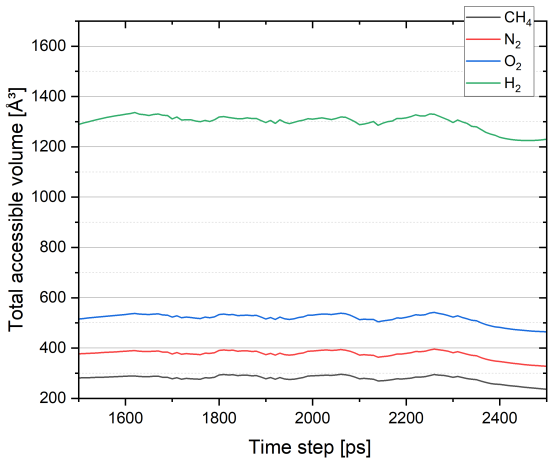

Figure 4.3: Total accessible volume [$Å^3$] of the sheared matrix

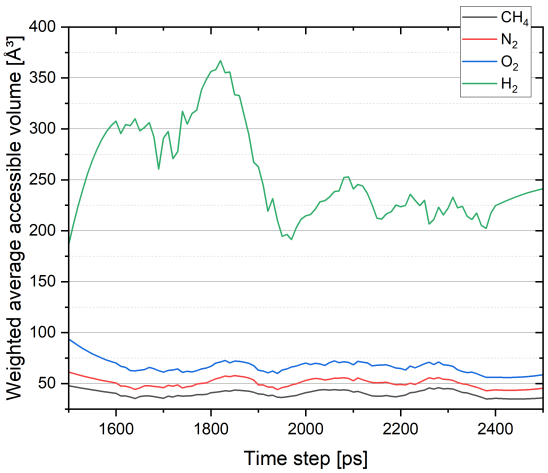

Figure 4.4: Weighted average cavity volume [$Å^3$] of the sheared matrix

4.2 | Final cavity results

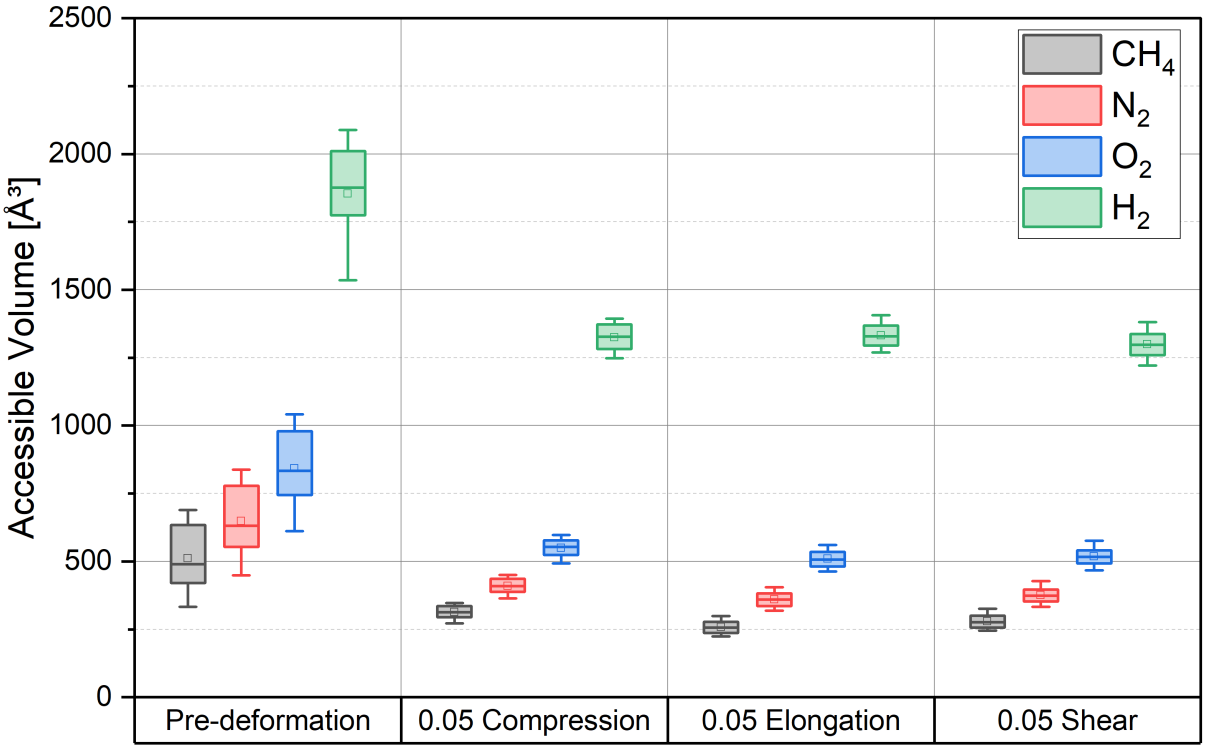

Figure 4.5: Box-plots with the accessible volumes Å^3 for each different molecule during the different deformation runs

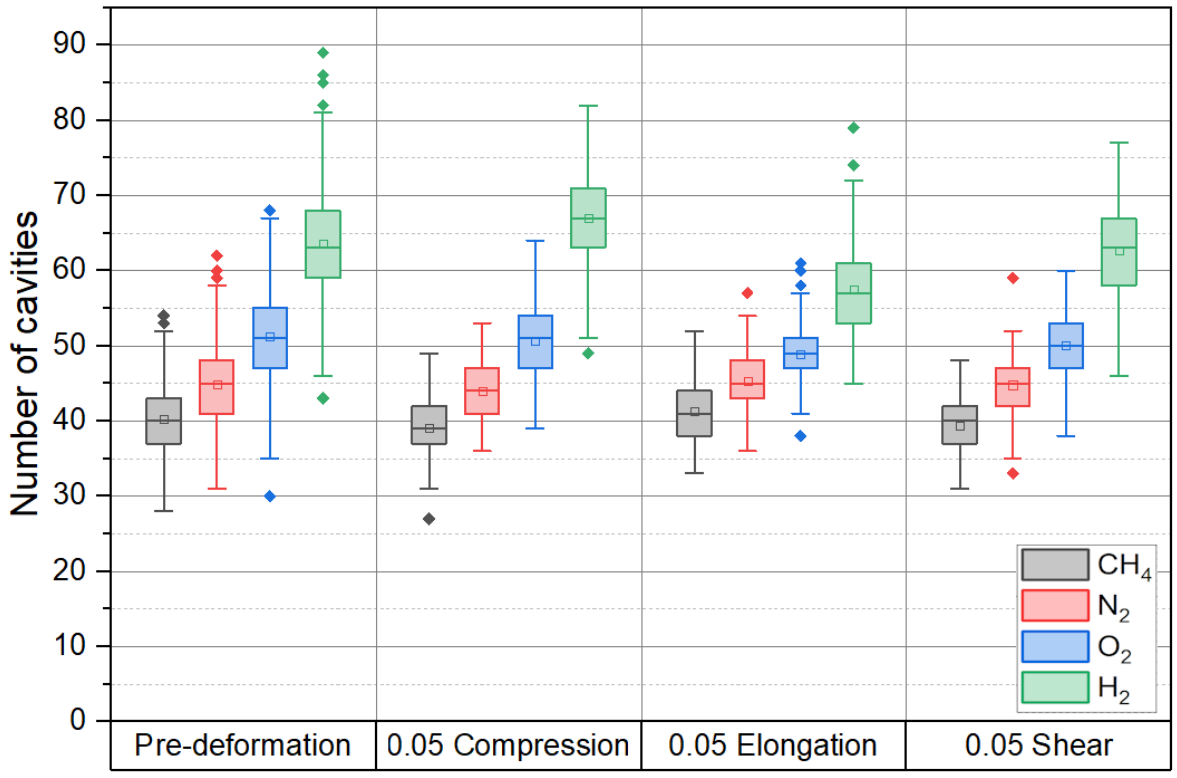

Figure 4.6: Box-plots with the different number of cavities for each different molecule during the different deformations runs

4.2.1 | Accessible volume

The above graphs showcase in a box-plot the total accessible volume Figure 4.5 and number of cavities Figure 4.6 for the different molecular penetrants prior to the deformation and after the deformation runs. As is evident from Figure 4.5, the total accessible volume between the chains decreases after each deformation has been applied. This means that the steady-states of the deformation-run configurations have less space accessible to molecular penetrants than during the undeformed steady-state. The accessible volumes' median and variances are close to identical after each of the deformations considering each different penetrant molecule. Of course, the accessible volumes for the different penetrants depends on the size of the molecules. Methane is the biggest molecule so it follows that it has a lower total accessible volume. But the ratio between the accessible volumes of the different molecules remains also close to identical before and after each of the deformations.
Another insight is that the undeformed configurations have roughly a 3.5 times higher standard deviation in accessible volumes than the deformation configurations. This means that the geometry of the configuration in the undeformed state is more unstable since the different polystyrene chains are more free to move with no deformation applied which results in some cavities growing and decreasing in size with a higher variance. Some cavities can disappear because the movement of the polystyrene chains blocks off access to any of the penetrant molecules as discussed in subsection 4.1. This also becomes evident from a visual inspection shown in Appendix A where the cavities change size and shape rapidly during what is an equilibrium trajectory of the undeformed configurations.

4.2.2 | Number of cavities

As opposed to the accessible volumes for each of the penetrants, the total number of cavities does not decrease after a deformation has been applied to the simulation cell as can be seen from Figure 4.6. But the smaller the molecule, the more accessible cavities it has. The variance of the number of cavities (especially in the undeformed configurations) is also higher for hydrogen because the smaller cavities are less stable. A small cavity can disappear or merge much more easily than the bigger cavities after a movement in the polystyrene chains.
Interestingly the elongation configurations contain more outliers than both the compression and shear configurations. But overall, the total number of penetrant accessible cavities remains largely the same for each respective molecule before and after the deformations.

4.2.3 | Big and small cavities

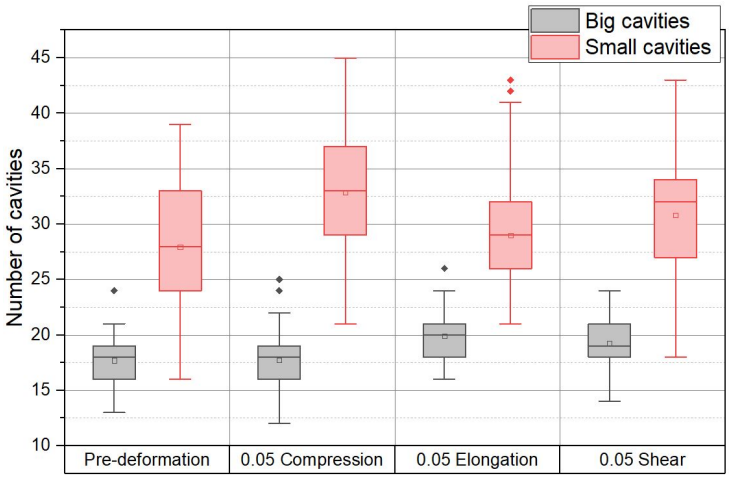

Figure 4.7: Cavity size comparison for oxygen accessible cavities regarding the different states

Figure 4.7 shows that there are around 1.5 times as many small cavities than big cavities for the different states. The configurations after compression have the highest variation in cavity sizes. But, overall the number of oxygen accessible cavity sizes is comparable for each of the states. Again, the higher variance in the number of small cavities shows that these are by nature more volatile, since they are more affected by movements of the polystyrene chains and can disappear or re-appear more easily than the bigger cavities.

5 | Solubility of the molecular penetrants

The newly formed cavity geometries resulting from the applied deformations to the equilibrium state of the polystyrene simulation cell might allow molecular penetrants to settle in between the polymeric chains as penetrants. The methodology to quantify the amount of potential penetrants is discussed in subsection 2.4. Below the relative volumetric solubility of the different penetrant gases is shown for each of the discussed deformation states.

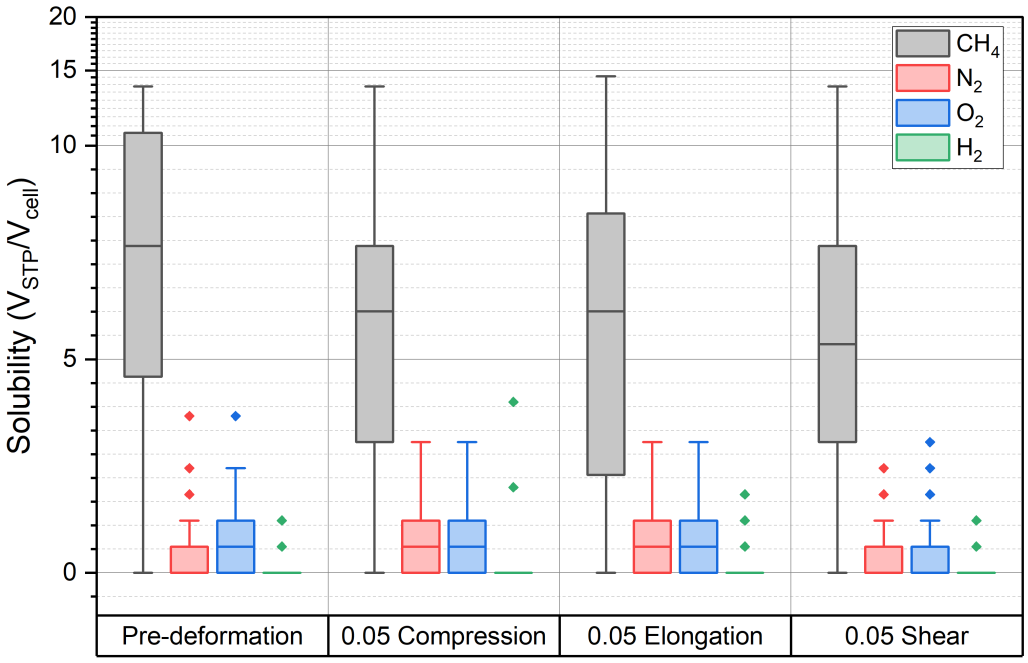

Figure 5.1: Solubility of the different molecular gases in each of the different states

Another alternative visualization of the relative solubilities over the pressure (1 *atm*) is shown in Appendix B. These particular results will later be used for a comparison to a previous study in subsection 5.1. The solubility of the different gases seems to be much more dependent on the specific characteristics of the molecular penetrant, than on the accessible volume available to it. Methane has a far lower accessible volume than hydrogen in all of the different states depicted in Figure 4.5, yet it solutes far easier into the polystyrene matrix. Even though these two molecules are both non-polar molecules, the size of the methane molecule might paradoxically make it easier to solute into the polystyrene because of its more favourable and more plentiful "van der Waals" interactions. Methane, having more electrons and a larger electron cloud compared to hydrogen, can engage in stronger London dispersion forces [13] (a type of "van der Waals" force) with the phenyl groups and the hydrocarbon parts of the polystyrene. These types of interactions are apparently well captured by the Lennard-Jones potentials in the OPLS-AA force field [8] employed during the GCMC-simulation from subsection 2.4. But a more thorough additional study would have to be conducted to describe these molecular interactions in more detail for each particular simulation cell to quantify the effect of the penetrants enviroment in solubility.
In each case there is no clear correlation between the accessible volume to a certain molecular penetrant and its solubility. It seems that the deformed/restricted configurations of the polystyrene with a lower accessible volume still have a very similar molecular penetrant solubility compared to the undeformed state. It might be that with another molecule that solubilizes even easier than methane, the accessible volume changes would be more of a factor in the total relative volumetric solubility because the inter-molecular forces and "van der Waals" interactions would become less relevant than the total accessible volume the penetrants can occupy before and after the deformation has been applied.
After all, the medians of the solubility of methane in each of the different deformed states of the simulation cell are very comparable with a difference of less than 10 %.
Another observation from Figure 5.1 is that in the compressed and elongated state the oxygen solubility is heightened with a median solubility of 0.5 of relative occupied volume in comparison to oxygen solubility in the undeformed state. Also, the nitrogen solubility is lower in the shear state than all the others. It seems that oxygen and nitrogen are comparable in their respective solubilities in each of the states due to

their comparable molecular sizes, non-polar nature, and similar interactions with the polymer structure. Nitrogen is the sligthly bigger molecule however and this might explain why its overall solubility is lower in the poylstyrene matrix.
But again, these observations can only be explained by doing a thorough analysis into the molecular interactions between polystyrene and these molecular penetrants. This could potentially be done with a focus on hydrogen because it has by far the lowest solubility of all the tested molecular gases. The median of the hydrogen solubility for each state is zero. Only in the compression state are there significant outliers going up to 4 relatively occupied volume.
Overall, no matter the particular deformation state, methane has the highest solubility with nitrogen and oxygen being comparable in their solubilities while hydrogen almost never solutes at all between the polystyrene chains.

5.1 | Comparison to experimental data

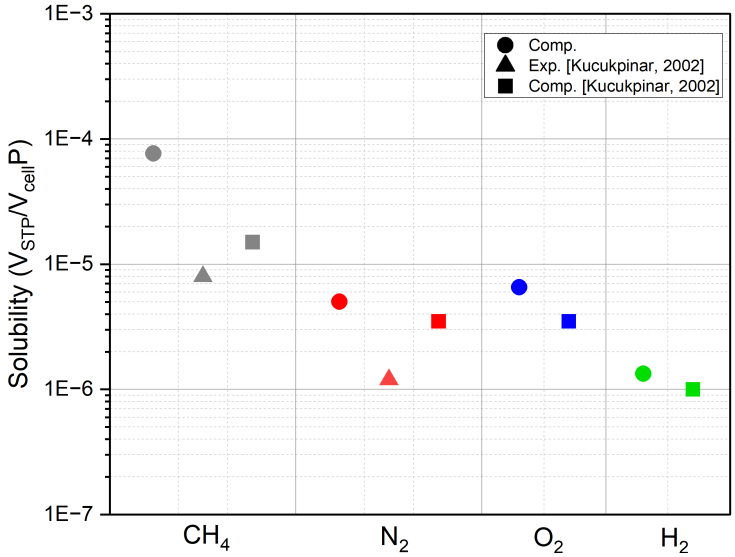

Figure 5.2: Box-plots of the computational (Comp.) relative volumetric solubility in the pre-deformation state from section 5 along the computional and experimental results (Exp.) from (Kucukpinar, 2002 [5])

Figure 5.2 showcases that the results from these GCMC-simulations for the equilibrated relative volumetric solubility in the undeformed state allign with experimental and computational results [5]. The solubility metric is divided by the pressure (1 *atm*) for a one-to-one comparison. This further validates the results of the approach employed. Kucukpinar et alli provide no experimental data for the solubility of hydrogen and oxygen. However, the computational results of that paper indicate similar trends for the relative solubilities of the molecules discussed in this report. Methane has the highest solubility, followed then by oxygen, nitrogen and finally hydrogen which has the lowest. The magnitude of the solubility was divided by the pressure which is at 1 *bar* for a clear comparison.

6 | Affine elongation comparison

A final consideration is the fact that there could be an easier way to get the cavity geometries of each of the deformed states. This new method could be conducted by applying a deformation tensor on the individual atoms in the polystyrene simulation cell to achieve an affine deformation. An affine deformation assumes that the local strain in a sample after deformation is identical everywhere and equal to the macroscopic strain [14]. If the simulation cell would deform in an affine manner it is not necessary to sample configurations from an MD-simulation [6] since the considered parameters and constraints in such a simulation would not affect the cavity geometry significantly. This same affine deformation tensor is also to be applied to the simulation cell itself such that the cavity searching algorithm from subsection 2.2 can be used appropriately after the all the atoms have been displaced. The following deformation tensor is applied to both the simulation cell and the polystyrene matrix:

$$\mathbf{F} = \begin{bmatrix} \lambda & 0 & 0 \\ 0 & \frac{1}{\lambda^2} & 0 \\ 0 & 0 & \frac{1}{\lambda^2} \end{bmatrix} = (\nabla_0 \vec{x})^T \tag{6.1}$$

where λ stands for the stretch factor which is 1.05 for an elongation in the case of a 0.05 strain being applied [15]. This deformation tensor is then applied to the positions of the atoms where the new atom positions are calculated through:

$$d\vec{x} = \mathbf{F} \cdot d\vec{X} \tag{6.2}$$

where $\vec{x}$ and $\vec{X}$ are the new and old atom positions respectively. The configuration on which this deformation is applied is the latest configuration of the undeformed state. After the deformation has been applied, the cavity searching algorithm is used on this affine configuration. And after the cavities have been identified, the voxel positions of the affine cavity configuration are compared to the voxel positions of the earliest configuration of the elongation state which was achieved through an actual MD-simulation (subsection 2.1). This would be called the "real" geometric configuration. This comparison is done through a k-d tree algorithm, which is a data structure used for organizing points in a dimensional space which is in this case is the cavity geometry. [16].

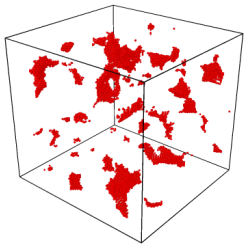

Figure 6.1: Cavity geometry of the "real" elongation configuration

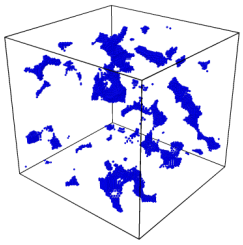

Figure 6.2: Cavity geometry of the affine elongation configuration

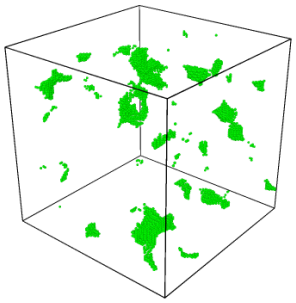

Figure 6.3: Cavity geometry of the matching voxels between the two configurations

This algorithm outputs the voxels of the "real" elongation configuration which are as close or closer than 0.5 Å^3 in distance to the voxels of the affine configuration. These voxels are both in the "real" and affine configurations. This new configuration can be seen in Figure 6.3.
The new collection of the matching voxels has a 54.5% similarity to the "real" geometric configuration. A difference this big makes this "affine" method of creating the deformed states of the polystyrene matrix for the evaluation of the penetrant accessible volume suboptimal and not representative of the actual results. This affine deformation method could be used as a very quick way of getting an idea of the resulting cavity geometry after a deformation is applied to a simulation cell without running an MD-simulation. But the bond constraints and dynamics [6] considered in the MD-simulations have a great influence on the polystyrene matrix configuration and therefore also influence the resulting cavity geometry.

7 | Conclusion

The study presented in this report has brought to light the differences in nano-cavity geometries and gaseous penetrant solubilities inside atactic polystyrene before and after mechanical deformations (compression, elongation and shear) of 0.05 strain were applied to it. These properties were analyzed through the use of Molecular Dynamics simulations [6] as a computational method with the OPLS-AA force field [8]. The atactic polystyrene [4] was simulated in the program "Large-scale Atomic/Molecular Massively Parallel Simulator" in the form of four polystyrene chains in a simulation cell with periodic boundary conditions. A cavity searching algorithm (subsection 2.2)was applied such that the nano-cavity geometry of the configurations sampled from these MD-runs could be identified for four different molecules; methane, nitrogen, oxygen and hydrogen before and after the deformations were applied. Accessible volumes for these different molecules are directly related to their respective sizes shown in Table 2.1. A smaller penetrant molecule has more accessible volume and overall more cavities accessible to it in the polystyrene matrix. The different deformations all restrict the total accessible volumes to each of molecules but the type of deformation does not seem to change the restriction in accessible volume (subsection 4.2). After a deformation has been applied to the matrix, the cavity geometry becomes more stable because the total accessible volume has a much smaller variance (Figure 4.5). Especially smaller cavities are considered unstable since they appear and disappear more frequently than the bigger cavities (Figure 4.7). Deforming the matrix does not affect the number of cavities however (Figure 4.6), so after a deformation has been applied to the matrix all of the cavities seem to shrink in size. It is the vibrational movement of the polystyrene chains which causes these fluctuations in geometry [12]. By assuming an affine deformation (section 6) with a deformation tensor on the polystyrene matrix another method for finding the cavity geometries was tested. In this method no MD-simulations were used but overall the end-results of the cavity geometry seem to be very much influenced by the dynamics and bond constraints considered in the MD-simulations, so using this method to acquire conclusive cavity-geometries seems ill-advised.
Another facet of this study was quantifying the molecular penetrant solubility of the mentioned gases in the matrix through a "Grand Canonical Monte Carlo" simulation (subsection 2.4). Molecular solubility seemed unaffected by the deformations on the matrix and was determined to be far more dependent on the individual characteristics and properties of the tested molecules (section 5). Even though methane had the lowest total accessible volume in all of the different deformation states it has the highest molecular solubility as a gas inside of the polystyrene matrix. The gases in order of solubility in the polystyrene matrix are methane, oxygen, nitrogen and then hydrogen which has a remarkably low solubility in polystyrene only rarely appearing in a few configurations. These solubilities were compared to experimental and computational results by E. Kucukpinar [5] and overall the different solubilities seem to align with these past results. But more research needs to be done to study the specific interactions occurring in the polystyrene with the gaseous penetrant molecules. This report can however be used as a reference for those potentially deepening studies.

7.1 | Recommendations

It would be to advisable to use another completely new polystyrene matrix for alternative configurations before and after the applied deformations to perform the same runs and algorithms on it as discussed in this report to hopefully arrive to the same conclusions. This would suffice as a (time-costly) but final validation of the results. Regarding this specific study, the thermal history could have also been studied where the polystyrene matrix would be equilibrated at different temperatures to see the effects of a temperature change on the cavity geometry and solubility, but sadly time constraints did not permit this. Also more types of molecular penetrants could have been tested in their cavity geometries and solubilities, as well as additional deformation configurations considering torsion and higher strains. Like previously mentioned in section 5 it would be very interesting to continue the studies of nano-porosity and molecular penetrant solubility in polystyrene by taking researching the interactions between the polystyrene and the molecular penetrants related to the total free accessible volume. For example, from past experiments conducted on the solubility of polystyrene it was determined that carbon dioxide has a far higher solubility than even methane [5], it would be interesting to see if this is also the case with another GCMC-run. Additionally other glassy systems could also be studied, polystyrene is one of many glassy polymers with industrial and academic relevance. And instead of the solubility, the diffusivity of penetrants through such glassy systems would also be an interesting study. Overall, the behaviour of nano-porous glassy systems exposed to deformations can still be explored far more both computationally and experimentally

8 | References

[1] R. J. Young and P. A. Lovell. *Introduction to polymers*. June 2011.

[2] D.J. Mulder. *Adjustable nanoporous polymers based on smectic liquid crystals*. PhD thesis, TU Eindhoven, October 2017.

[3] T. Guo-Liang, Z. Hui-Hsin and W Ming-Yen. Feasibility of using waste polystyrene as a membrane material for gas separation. *Chemical Engineering Research and Design*, March 2016.

[4] J.R. Wünsch. *Polystyrene: Synthesis, Production and Applications*. Rapra Technology Limited, 2000.

[5] E. Kucukpinar and P. Doruker. Molecular simulations of small gas diffusion and solubility in copolymers of styrene. *Polymer*, June 2002.

[6] M. P. Allen. Introduction to molecular dynamics simulation. *Computational Soft Matter: From Synthetic Polymers to Proteins*, January 2004.

[7] T. Wang, D. W. Heermann, and J.-C. Heilig. Diffusion of gas molecules in the polystyrene matrix. *Macromolecular theory and simulations*, December 2000.

[8] J. William. Development and testing of the opls all-atom force field on conformational energetics and properties of organic liquids. *Journal of the American Chemical Society*, November 1996.

[9] K. Qia, G. Xiaoting, L. Shouwei, D. Chongxiong, and Libo L. Effects of thermostats/barostats on physical properties of liquids by molecular dynamics simulations. *Journal of Molecular Liquids*, November 2022.

[10] Z. W Qiang W Fuyan D. Rufang Y. Kang, Y. Dunhong and K. Cai. Fully atomistic molecular dynamics computation of physico-mechanical properties of pb, ps, and sbs. *Nanomaterials*, July 2019.

[11] D. Frenkel. Introduction to monte carlo methods. *Computational Soft Matter: From Synthetic Polymers to Proteins*, March 2004.

[12] G. Sumpter W. Noid E. Tuzun Yang C. Bryan, C. Hathorn. Computational simulation of polymer particle structures: vibrational normal modes using the time averaged normal coordinate analysis method. *Polymer*, June 2003.

[13] J. Jansen G. Ángyán, J. Dobson and T. Gould. *London Dispersion forces in molecules, solids and nano-structures*. Royal Society of Chemistry, April 2020.

[14] Q. Wen, A. Basu, P. A. Janmey, and A. G. Yodh. Non-affine deformations in polymer hydrogels. *Soft matter*, January 2012.

[15] M. Geers. *Fundamentals and engineering concepts of elasticity-based design in mechanical engineering*. TU Eindhoven, December 2024.

[16] J.L. Bentley. Multidimensional binary search trees used for associative searching. *Commun. ACM*, September 1975.

A | Appendix - Oxygen accessible cavity geometry throughout the equilibrated state of the undeformed polystyrene matrix

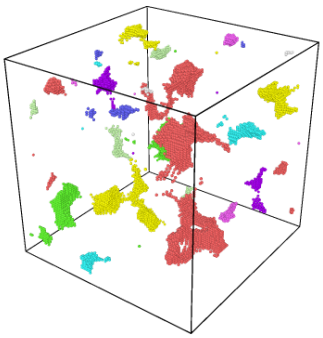

Oxygen accessible cavity geometry at 0 ns

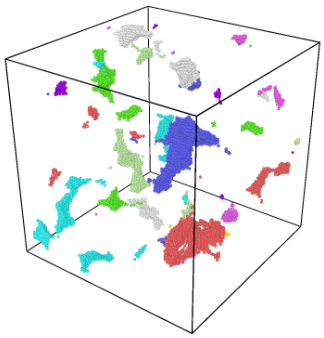

Oxygen accessible cavity geometry at 0.1 ns

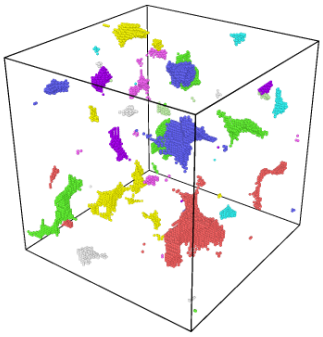

Oxygen accessible cavity geometry at 0.2 ns

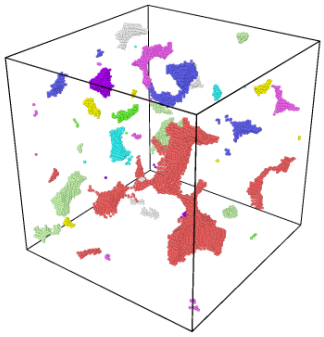

Oxygen accessible cavity geometry at 0.3 ns

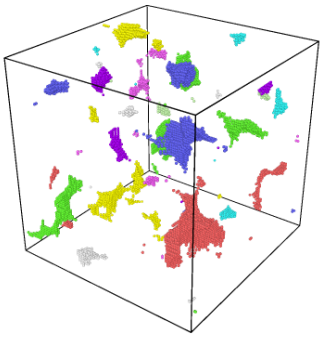

Oxygen accessible cavity geometry at 0.4 ns

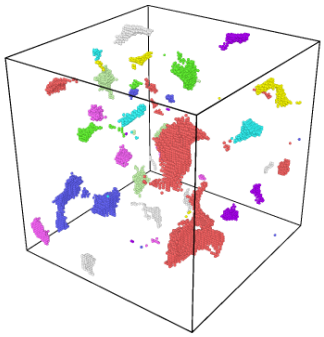

Oxygen accessible cavity geometry at 0.5 ns

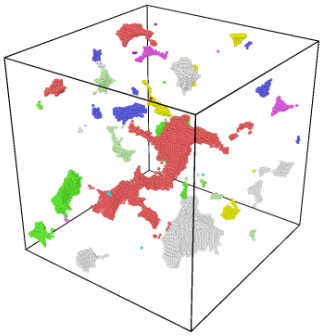

Oxygen accessible cavity geometry at 0.6 ns

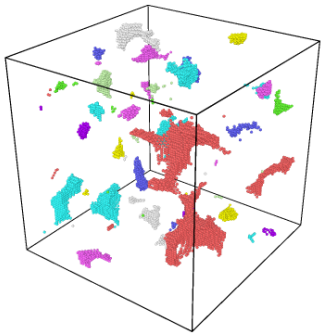

Oxygen accessible cavity geometry at 0.7 ns

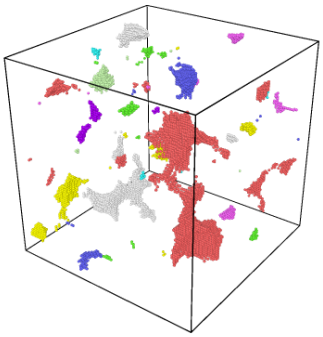

Oxygen accessible cavity geometry at 0.8 ns

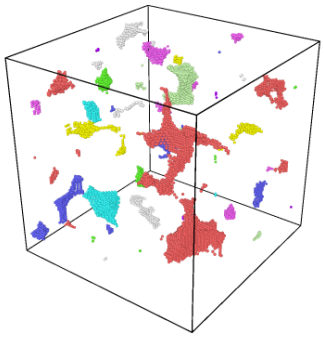

Oxygen accessible cavity geometry at 0.9 ns

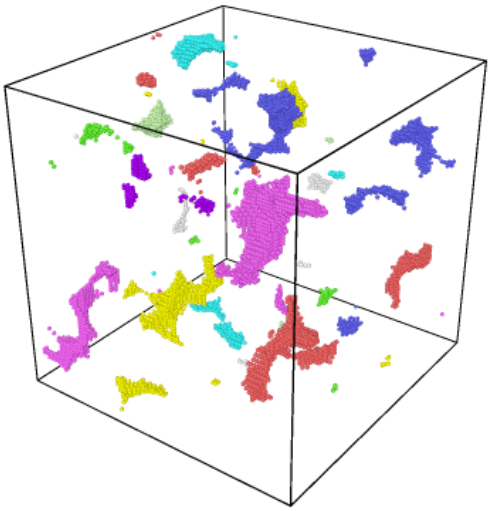

Final oxygen accessible cavity geometry at 1 ns

B | Appendix - Alternative visualization of the gaseous penetrant solubilities.

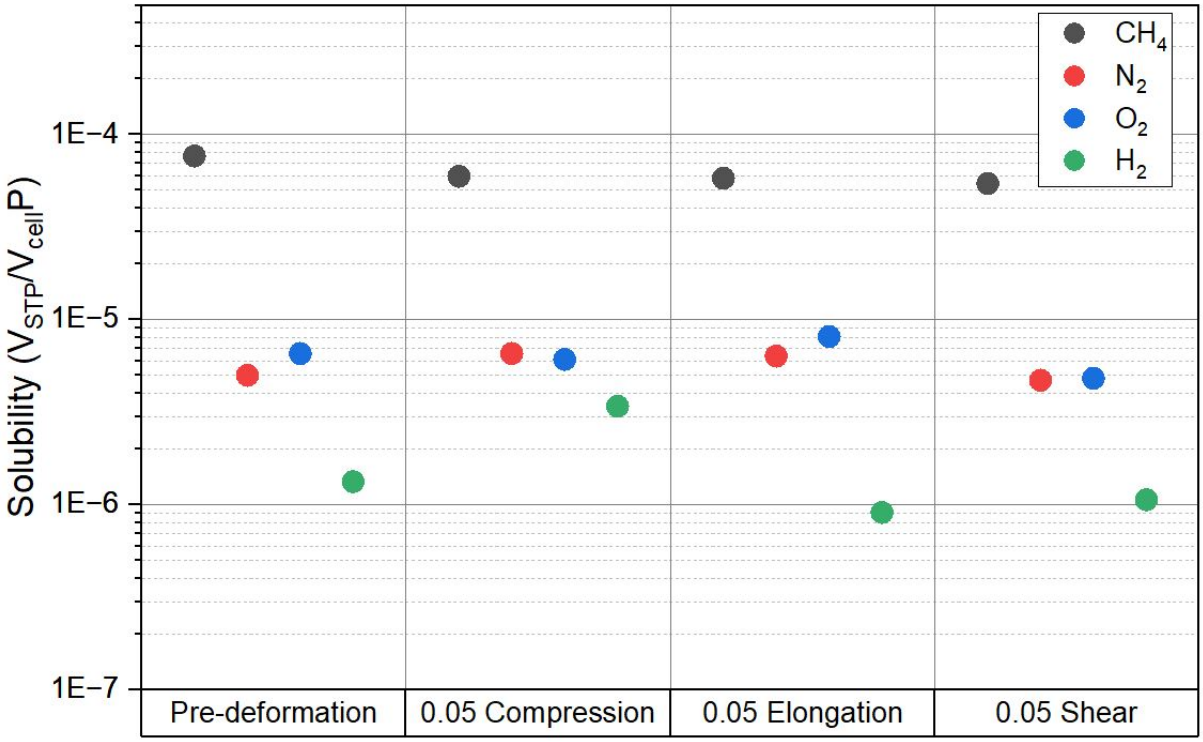

Figure B.1: The means of the different solubilities for each penetrant molecular gas in the different states, now divided by the pressure (1 atm)